COMMUNICATIONS IN COMPUTATIONAL PHYSICS
Vol. **4**, No. 4, pp. 911-928

Commun. Comput. Phys.
October 2008

The Method of Fundamental Solutions for Steady-State Heat Conduction in Nonlinear Materials

A. Karageorghis[1,*] and D. Lesnic[2]

[1] *Department of Mathematics and Statistics, University of Cyprus, 1678 Nicosia, Cyprus.*
[2] *Department of Applied Mathematics, University of Leeds, Leeds LS2 9JT, UK.*

Received 19 October 2007; Accepted (in revised version) 21 February 2008

Available online 29 May 2008

Abstract. The steady-state heat conduction in heat conductors with temperature dependent thermal conductivity and mixed boundary conditions involving radiation is investigated using the method of fundamental solutions. Various computational issues related to the method are addressed and numerical results are presented and discussed for problems in two and three dimensions.

AMS subject classifications: 65N35, 65N38, 65H10

Key words: Nonlinear heat conduction, radiation, method of fundamental solutions.

1 Introduction

Two-dimensional boundary value problems of heat conduction in nonlinear materials and nonlinear boundary conditions have been investigated using the boundary element method (BEM) by Bialecki and Nowak [3] and Ingham *et al.* [12]. However, the implementation of the BEM becomes rather tedious for problems in three-dimensional irregular domains. Moreover, the evaluation of the gradient of the temperature solution on the boundary requires the use of finite differences or the evaluation of hypersingular integrals. In order to alleviate some of these difficulties, this paper proposes the use of the method of fundamental solutions (MFS), a meshless Trefftz-type method which is considerably easier to implement. The advantages of the MFS over the finite difference method (FDM), the finite element method (FEM), and the BEM for solving elliptic boundary value problems, especially in higher-dimensions where no discretization of the solution domain, or its boundary, is necessary, are well-documented, see for example the survey papers [6,7,10].

*Corresponding author. *Email addresses:* andreask@ucy.ac.cy (A. Karageorghis), amt5ld@maths.leeds.ac.uk (D. Lesnic)

The MFS was first applied to potential flow problems by Johnston and Fairweather [13] and has since been applied to a large variety of physical problems. In this work, we shall employ the same idea of expressing the solution of the Laplace equation as a linear combination of fundamental solutions with singularities located outside the domain of the problem under consideration. In [14], Karageorghis and Fairweather used the MFS for solving linear material problems with nonlinear radiative boundary conditions. The purpose of this study is to extend this analysis to nonlinear material problems in two and three dimensions.

The mathematical formulation of the problem is given in Section 2 and the MFS description in Section 3. In the previous study of Karageorghis and Fairweather [14], the gradient of the nonlinear least-squares objective function which is minimized was calculated internally by default using 'blind' finite differences. Thus with perturbing the parameters one at a time, the Jacobian matrix is recalculated at every iteration. Therefore, the finite-difference approach for calculating the gradient has a high computational cost, see Rus and Gallego [25]. In order to save on the computational time the Jacobian matrix is calculated analytically. Numerical results are compared with the BEM results of Bialecki and Nowak [3] for two test examples in Section 4. Moreover, a three-dimensional example is considered, apparently, for the first time. Finally, comments and conclusions are presented in Section 5.

2 Mathematical formulation

We consider a simply-connected bounded domain $\Omega\subset\mathbb{R}^d$, $d\geq 2$, with piecewise smooth boundary $\partial\Omega$ and assume that this boundary is composed of three disjoint parts Γ_1, Γ_2 and Γ_3. On each part Γ_i,$i=1,2,3$ boundary conditions of the first (Dirichlet), second (Neumann) and third (Robin) kind, respectively, hold. The mathematical problem governing steady-state heat conduction is given by, see [3],

$$\nabla\cdot(k(T)\nabla T)=0 \quad \text{in} \quad \Omega, \tag{2.1}$$

subject to the boundary conditions

$$T=f \quad \text{on} \quad \Gamma_1, \tag{2.2a}$$

$$-k(T)\frac{\partial T}{\partial n}=g \quad \text{on} \quad \Gamma_2, \tag{2.2b}$$

$$k(T)\frac{\partial T}{\partial n}+h\left[T-T_f\right]+C_0R\left[T^4-T_s^4\right]=q \quad \text{on} \quad \Gamma_3, \tag{2.2c}$$

where T is the temperature solution, k is the thermal conductivity, $\boldsymbol{n}$ is the unit outward normal vector to the boundary $\partial\Omega$, f is a prescribed temperature on the boundary Γ_1, g is a prescribed heat flux on the boundary Γ_2 and q is a given function on the boundary Γ_3 which is usually taken to be zero. Also, h is the convective heat transfer coefficient, T_f is

the temperature of fluid exchanging heat with Γ_3, $C_0=5.667\times10^{-8}\,W/m^2K^4$ is the Stefan-Boltzman constant, R is the radiation interchange factor (emissivity) between the boundary Γ_3 and the environment, having a temperature T_s, and, for simplicity, no heat sources are assumed present. In boundary condition (2.2c), the nonlinearity occurs mainly due to heat radiation although the method of solution can also allow nonlinearities occurring from the temperature dependent heat transfer coefficient h or from the temperature dependent radiation interchange factor R.

The nonlinear governing partial differential equation (2.1) can be easily transformed into the Laplace equation by employing the classical Kirchhoff transformation defined as, see, e.g., Özişik [22],

$$\Psi=\psi(T):=\int_0^T\frac{k(\xi)}{k_0}d\xi, \tag{2.3}$$

where $k(T)=k_0(1+m(T))$, k_0 is a positive constant and $m(T)>-1$ is a known function. This expression for $k(T)$ is useful in order to highlight the deviation of $k(T)$ from a uniform (constant) thermal conductivity k_0. Since $k>0$, the inverse transformation to (2.3) exists and is given by

$$T=\psi^{-1}(\Psi). \tag{2.4}$$

Efficient techniques for performing Kirchhoff's transformation (2.3) and its inverse (2.4) may be found in Azevedo and Wrobel [2]. It follows from (2.3) that

$$k(T)\nabla T=k_0\nabla\Psi.$$

Then problem (2.1)-(2.2) transforms into the equivalent form

$$\nabla^2\Psi=0 \quad \text{in} \quad \Omega, \tag{2.5}$$

subject to the boundary conditions

$$\Psi=\psi(f) \quad \text{on} \quad \Gamma_1, \tag{2.6a}$$

$$-k_0\frac{\partial\Psi}{\partial n}=g \quad \text{on} \quad \Gamma_2, \tag{2.6b}$$

$$k_0\frac{\partial\Psi}{\partial n}+h[\psi^{-1}(\Psi)-T_f]+C_0R[\psi^{-1}(\Psi)^4-T_s^4]=q \quad \text{on} \quad \Gamma_3. \tag{2.6c}$$

In the above boundary value problem the only nonlinear equation is the one corresponding to the boundary condition on Γ_3. It can be shown that under certain assumptions on f, g, q, k and h, problem (2.5)-(2.6) has a unique solution, see Ruotsalainen and Wendland [23]. Once Ψ is found, T is readily determined from (2.4), via (2.3).

3 The method of fundamental solutions (MFS)

In the MFS (see, for example [5, 20]), the approximation for the solution $\Psi(\boldsymbol{x})$ of the boundary value problem (2.5)-(2.6) has the form

$$\Psi_{\mathcal{N}}(\boldsymbol{c};\boldsymbol{x})=\sum_{j=1}^{\mathcal{N}}c_jG_d(\boldsymbol{\xi}_j;\boldsymbol{x}),\quad \boldsymbol{x}\in\overline{\Omega}=\Omega\cup\partial\Omega, \tag{3.1}$$

where $\mathcal{N}$ is the number of unknown *singularities (sources)*, $\boldsymbol{\xi}_j\notin\overline{\Omega}$, $(c_j)_{j=1}^{\mathcal{N}}$ are unknown real coefficients and G_d is a fundamental solution of the Laplace equation, given by

$$G_d(\boldsymbol{\xi}_j;\boldsymbol{x})=\begin{cases} -\dfrac{1}{2\pi}\log|\boldsymbol{\xi}_j-\boldsymbol{x}|, & d=2,\\ \dfrac{1}{4\pi}\dfrac{1}{|\boldsymbol{\xi}_j-\boldsymbol{x}|}, & d=3,\end{cases} \tag{3.2}$$

where $\boldsymbol{\xi}_j=(\xi_1^{(j)},\cdots,\xi_d^{(j)})$ and $\boldsymbol{x}=(x_1,\cdots,x_d)$.

The coordinates of the singularities may be either preassigned or let free and determined as part of the solution [6]. In this study, we adopt the former option where the singularities are fixed. Therefore, in Eq. (3.1) there are $\mathcal{N}$ unknowns, namely, the $\mathcal{N}$ coefficients c_j. These can be determined by imposing the boundary conditions (2.6a)-(2.6c) at $\mathcal{M}\geq\mathcal{N}$ distinct collocation points $(\boldsymbol{x}_i)_{i=1}^{\mathcal{M}}$ on the boundary $\partial\Omega$. Denoting the boundary points on each of the three parts of the boundary by $(\boldsymbol{x}_i)_{i=1}^{\mathcal{M}_1}\in\Gamma_1$, $(\boldsymbol{x}_i)_{i=\mathcal{M}_1+1}^{\mathcal{M}_2}\in\Gamma_2$ and $(\boldsymbol{x}_i)_{i=\mathcal{M}_2+1}^{\mathcal{M}}\in\Gamma_3$, we minimize the nonlinear least-squares objective function

$$\begin{aligned} S(\boldsymbol{c}):=&\sum_{i=1}^{\mathcal{M}_1}[\Psi_{\mathcal{N}}(\boldsymbol{c};\boldsymbol{x}_i)-\psi(f(\boldsymbol{x}_i))]^2+\sum_{i=\mathcal{M}_1+1}^{\mathcal{M}_2}\left[-k_0\frac{\partial\Psi_{\mathcal{N}}}{\partial n}(\boldsymbol{c};\boldsymbol{x}_i)-g(\boldsymbol{x}_i)\right]^2\\ &+\sum_{i=\mathcal{M}_2+1}^{\mathcal{M}}\Big\{k_0\frac{\partial\Psi_{\mathcal{N}}}{\partial n}(\boldsymbol{c};\boldsymbol{x}_i)+h(\boldsymbol{x}_i)[\psi^{-1}(\Psi_{\mathcal{N}}(\boldsymbol{c};\boldsymbol{x}_i))-T_f(\boldsymbol{x}_i)]\\ &+C_0R(\boldsymbol{x}_i)\left[\psi^{-1}(\Psi_{\mathcal{N}}(\boldsymbol{c};\boldsymbol{x}_i))^4-T_s^4(\boldsymbol{x}_i)\right]-q(\boldsymbol{x}_i)\Big\}^2. \end{aligned} \tag{3.3}$$

The minimization of (3.3) is carried out using the MINPACK [8] routines `lmdif` and `lmder`. The routine `lmdif` minimizes the sum of the squares of $\mathcal{M}$ nonlinear functions in $\mathcal{N}$ variables by a modification of the Levenberg-Marquardt algorithm. In it, the user must provide a subroutine which calculates the functions while the Jacobian matrix is calculated internally by a forward-difference approximation. In `lmder` the user must also provide the Jacobian matrix. More precisely, if we write the functional (3.3) in the simplified form $S(\boldsymbol{c})=\sum_{i=1}^{\mathcal{M}}[H_i(\boldsymbol{c})]^2$, then we need to provide the Jacobian matrix $J_{ij}=\partial H_i/\partial c_j, i=1,\cdots,\mathcal{M}, j=1,\cdots,\mathcal{N}$.

In the examples considered in this study we experimented with the ratio of boundary points $\mathcal{M}$ and sources $\mathcal{N}$. It was observed that the use of more boundary points than sources did not improve the accuracy of the MFS approximations substantially. Also, it was also observed, after extensive experimentation, that `lmder` reached a prescribed accuracy more rapidly than `lmdif`.

When using `lmder` we provided the Jacobian matrix J given as follows: For $j=1,2,\cdots,\mathcal{N}$,

$$J_{ij}=\begin{cases} G_d(\boldsymbol{\xi}_j;\boldsymbol{x}_i), & i=1,\cdots,\mathcal{M}_1, \\ -k_0\dfrac{\partial G_d}{\partial n(\boldsymbol{x})}(\boldsymbol{\xi}_j;\boldsymbol{x}_i), & i=\mathcal{M}_1+1,\cdots,\mathcal{M}_2, \\ k_0\dfrac{\partial G_d}{\partial n(\boldsymbol{x})}(\boldsymbol{\xi}_j;\boldsymbol{x}_i)+\dfrac{G_d(\boldsymbol{\xi}_j;\boldsymbol{x}_i)}{\psi'(\psi^{-1}(\Psi_N(\boldsymbol{c};\boldsymbol{x}_i)))} & \\ \times\left[h(\boldsymbol{x}_i)+4C_0R(\boldsymbol{x}_i)\psi^{-1}(\Psi_N(\boldsymbol{c};\boldsymbol{x}_i))^3\right], & i=\mathcal{M}_2+1,\cdots,\mathcal{M}. \end{cases} \tag{3.4}$$

A crucial question in the implementation of the MFS is the positioning of the pseudo-boundary on which the sources are to be placed. One way of dealing with this problem is to, as mentioned earlier in this section, let the singularities free to be determined as part of the solution [6]. This approach can, however, prove to be costly and has the serious drawback that, as the problem is highly nonlinear, there might be several minima in the non-linear least-squares minimization process to which the routine might converge. In this work, we fixed the singularities on a pseudo-boundary similar to boundary of the original domain (as recommended in [11]) and at a distance ε from it. In order to obtain an optimal ε we adopted an approach proposed in [27], in which the problem was solved, for each $\mathcal{N}$, for various values of $\varepsilon_\ell=\varepsilon_0+\ell\delta, \ell=0,1,\cdots,L$. For each ε_ℓ, the maximum error in the boundary conditions at a selected set of uniformly spaced points on the boundary (different from the boundary collocation points) was calculated. A good estimate for the optimal ε is to select the one for which the maximum error in the boundary conditions is minimized.

At present, there is no theoretical justification that sustains the above nonlinear minimization procedure in terms of convergence. However, this may be attempted in a future study by relating to the convergence and stability MFS numerical analysis provided in, for e.g., [5, 16–21, 26, 28].

4 Numerical results and discussion

In this section, we present numerical results obtained from the application of the MFS described in the previous section to some two and three-dimensional nonlinear heat transfer problems.

4.1 Example 1

We consider an example from Bialecki and Nowak [3] for a nonlinear material, but with linear convective boundary conditions and no radiation on Γ_3, i.e., $R=0$ in (2.2c). More precisely, a two-dimensional steady-state temperature field in the unit square $\Omega=(0,1)\times(0,1)$ is to be determined. The thermal conductivity is assumed to vary linearly with the temperature as

$$k(T)=k_0(1+m(T))=1\cdot(1+aT)\,W/mK, \tag{4.1}$$

where $a\geq 0$ is a prescribed constant. We take, see Fig. 1,

$$\Gamma_1=\{1\}\times[0,1],\quad \Gamma_2=\{0\}\times[0,1]\cup(0,1)\times\{0\},\quad \Gamma_3=(0,1)\times\{1\}, \tag{4.2}$$

$$f=300\,K,\quad h=10\,W/mK^2,\quad T_f=500\,K,\quad g=q=R=0. \tag{4.3}$$

Employing transformation (2.3) yields

$$\Psi=\psi(T)=T+\frac{aT^2}{2}, \tag{4.4}$$

with its inverse (2.4) given by

$$T=\psi^{-1}(\Psi)=\frac{-1+\sqrt{1+2a\Psi}}{a}, \tag{4.5}$$

where the negative root is discarded since $k(T)=1+aT$ has to be positive. Then the problem (2.5)-(2.6) becomes

$$\nabla^2\Psi=0\quad\text{in}\quad(0,1)\times(0,1), \tag{4.6}$$

subject to the boundary conditions

$$\Psi(1,x_2)=300(1+150a),\quad x_2\in[0,1], \tag{4.7a}$$

$$\frac{\partial\Psi}{\partial x_1}(0,x_2)=0,\quad x_2\in[0,1], \tag{4.7b}$$

$$\frac{\partial\Psi}{\partial x_2}(x_1,0)=0,\quad x_1\in(0,1), \tag{4.7c}$$

$$\frac{\partial\Psi}{\partial x_2}(x_1,1)+10\left[\frac{2\Psi(x_1,1)}{1+\sqrt{1+2a\Psi(x_1,1)}}-500\right]=0,\quad x_1\in(0,1). \tag{4.7d}$$

We first solve the problem with $a=0$. In this case $k(T)=1$ and there is no need to employ transformation (4.4), the problem to be solved being linear and given by

$$\nabla^2 T=0\quad\text{in}\quad(0,1)\times(0,1), \tag{4.8}$$

subject to the boundary conditions

$$T(1,x_2)=300, \quad x_2\in[0,1], \tag{4.9a}$$

$$\frac{\partial T}{\partial x_1}(0,x_2)=0, \quad x_2\in[0,1], \tag{4.9b}$$

$$\frac{\partial T}{\partial x_2}(x_1,0)=0, \quad x_1\in(0,1), \tag{4.9c}$$

$$\frac{\partial T}{\partial x_2}(x_1,1)+10(T(x_1,1)-500)=0, \quad x_1\in(0,1). \tag{4.9d}$$

We choose M uniformly distributed collocation points on each side of the square and N uniformly distributed source points on the pseudo-boundary which was taken to be a square of side $1+2\varepsilon$, i.e., a square similar to our domain and at a distance ε from it. Thus, in this case, $\mathcal{M}=4M$ and $\mathcal{N}=4N$.

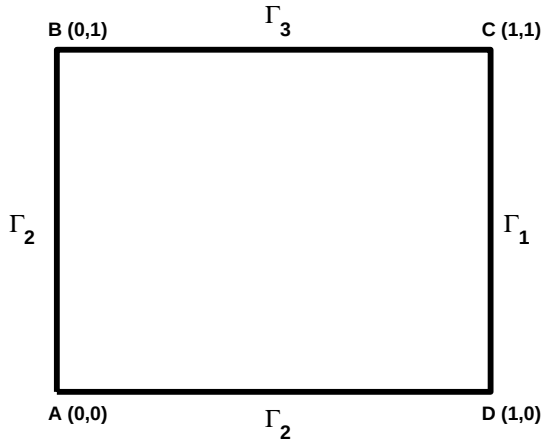

Figure 1: Geometry for Example 1.

In Fig. 2, we present the boundary temperature along the perimeter of the square for problem (4.8)-(4.9), starting from the origin and oriented clockwise in the case $a=0$ and obtained using $N=M=32$. From the physical point of view, the boundary temperature distribution has an expected monotonic variation on the insulated parts of the heat conductor. This figure compares (graphically) well with the corresponding figure from Bialecki and Nowak [3] obtained using the BEM.

In Fig. 3, we present the boundary temperature for $a\in\{0.1,0.3,0.5\}$ and obtained using $N=M=32$. The results for $a=0.3$ agree well with the corresponding results of Akella and Katamraju [1].

In Fig. 4 we present the error in the temperature along the side Γ_1 for the nonlinear cases $a=0.1,0.3,0.5$ using $N=M=32$. As can be seen the accuracy of these results is very good and appears to increase with increasing the value of a.

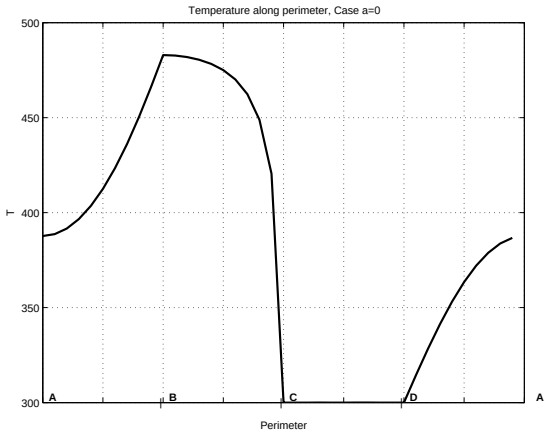

Figure 2: The boundary temperature along the perimeter of the unit square for the linear case $a=0$.

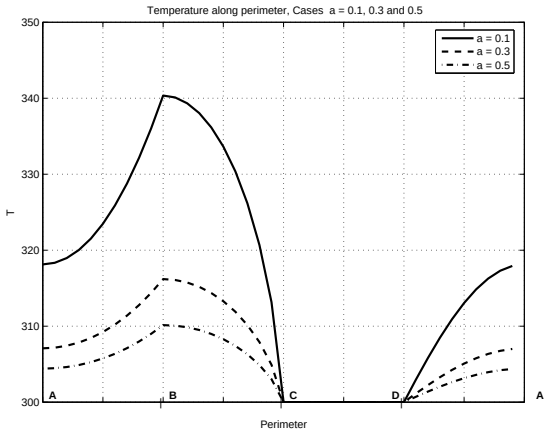

Figure 3: The boundary temperature along the perimeter of the unit square for the nonlinear cases $a=0.1,0.3,0.5$.

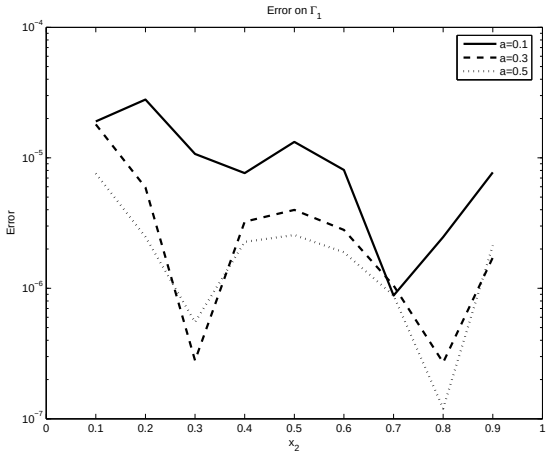

Figure 4: Error in temperature along the side Γ_1 for the nonlinear cases $a=0.1,0.3,0.5$.

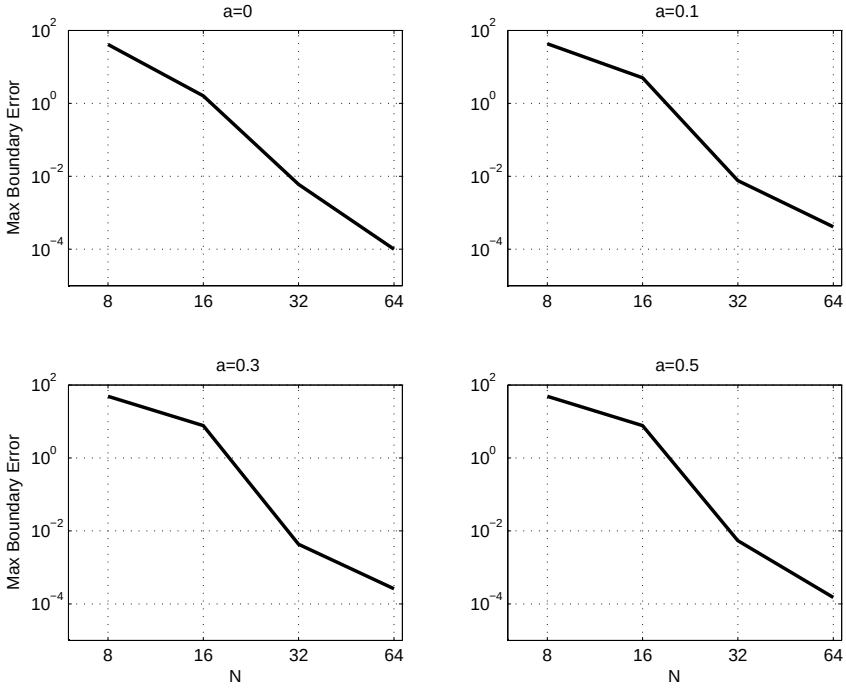

Figure 5: Maximum boundary errors with $N=M$ for the cases $a=0,0.1,0.3,0.5$.

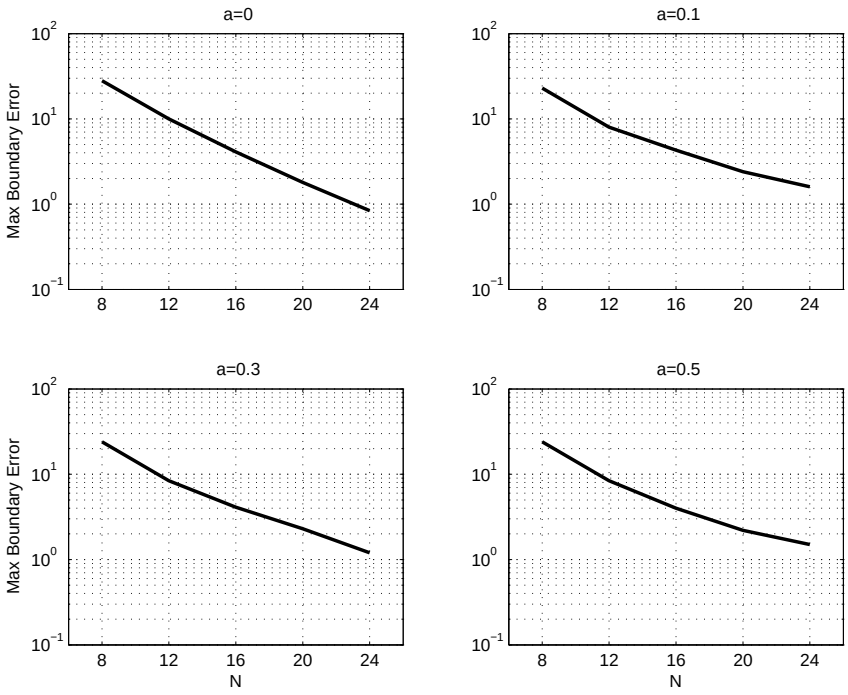

Figure 6: Maximum boundary errors with $N=M/2$ for the cases $a=0,0.1,0.3,0.5$.

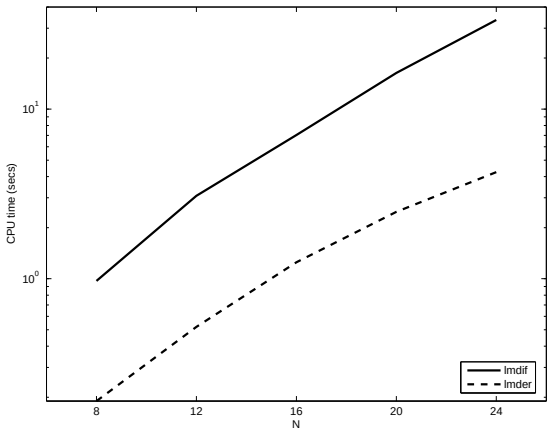

Figure 7: CPU times with $N=M/2$ for the case $a=0.1$.

In Fig. 5, we present the maximum error in the boundary conditions calculated at 40 uniformly spaced boundary points, for $N=M=8,16,32$ and 64, in the cases $a\in\{0,0.1,0.3,0.5\}$. As can be observed from these plots, there is an indication of exponential convergence of the error to zero with increasing N. This is in agreement with the theoretical studies of [15,17], although numerical round-off errors may affect the stability of the numerical results since the ill-conditioning of the MFS system increases with increasing $M(\geq N)$. If such a situation occurs, regularization of the ill-conditioned system is recommended, see [24]. It is noteworthy that the profiles of the temperature along the boundary were indistinguishable for values of $N\geq 12$. In Fig. 6, we present the maximum error in the boundary conditions calculated at 40 uniformly spaced boundary points, for $N=M/2=8,12,16,20$ and 24, in the cases $a\in\{0,0.1,0.3,0.5\}$. It appears that the use of more boundary points than sources does not improve substantially the accuracy of the MFS approximation.

In Fig. 7, we present the CPU times, in seconds, required by the routines `lmdif` and `lmder` to reach a prescribed accuracy in the case $a=0.1$ as $N=M/2$ takes the values 8,12,16,20 and 24. These times, which were recorded on an `IBM RS6000-F80` machine, show that the routine `lmder` leads to substantial savings in CPU time.

4.2 Example 2

We now consider a nonlinear material with the thermal conductivity given by

$$k(T)=k_0(1+aT),\quad k_0=1W/mK,\quad a=0.25K^{-1}, \tag{4.10}$$

occupying part of a cross-section of an industrial furnace, as depicted in Fig. 8. Linear convective boundary conditions with a constant heat transfer coefficient $h=40W/m^2K$, but with non-zero thermal radiation interchange factor $R=0.7$, are considered.

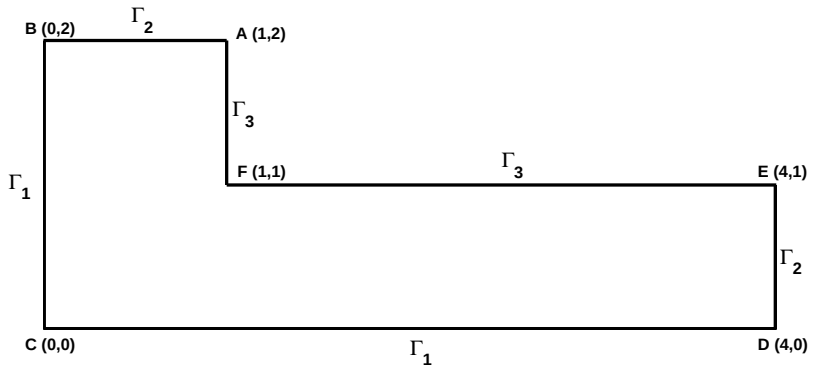

Figure 8: Geometry for Example 2.

We take, see Fig. 8,

$$\begin{aligned}&\Gamma_1=\{0\}\times[0,2]\cup(0,4)\times\{0\},\quad \Gamma_2=(0,1)\times\{2\}\cup\{4\}\times[0,1],\\&\Gamma_3=(1,4)\times\{1\}\cup\{1\}\times[1,2],\end{aligned}\tag{4.11}$$

and $f=320\,K$, $T_f=500\,K$, $T_s=1000\,K$, $g=q=0$. Employing transformation (4.4), problem (2.5)-(2.6) becomes

$$\nabla^2\Psi=0\quad\text{in}\quad\Omega,\tag{4.12}$$

subject to the boundary conditions

$$\Psi(0,x_2)=\Psi(x_1,0)=13120,\quad x_1\in(0,4),\quad x_2\in[0,2],\tag{4.13a}$$

$$\frac{\partial\psi}{\partial x_2}(x_1,2)=\frac{\partial\psi}{\partial x_1}(4,x_2)=0,\quad x_1\in(0,1),\quad x_2\in[0,1],\tag{4.13b}$$

$$\frac{\partial\Psi}{\partial x_2}(x_1,1)+p(x_1,1)=0,\quad x_1\in(1,4),\tag{4.13c}$$

$$\frac{\partial\Psi}{\partial x_2}(1,x_2)+p(1,x_2)=0,\quad x_2\in[1,2],\tag{4.13d}$$

where

$$\begin{aligned}p(x_1,x_2)=&160\left[\sqrt{1+0.5\Psi(x_1,x_2)}-126\right]\\&+3.967\times10^{-8}\left[256\Big(-1+\sqrt{1+0.5\Psi(x_1,x_2)}\Big)^4-10^{12}\right].\end{aligned}$$

We choose M uniformly distributed collocation points on the sides DE, AF and AB, $2M$ points on the side BC, $3M$ points on the side EF, and $4M$ points on the side CD. On the pseudo-boundary the sources were distributed in a similar way with N replacing M. Thus, in this case $\mathcal{M}=12M$ and $\mathcal{N}=12N$.

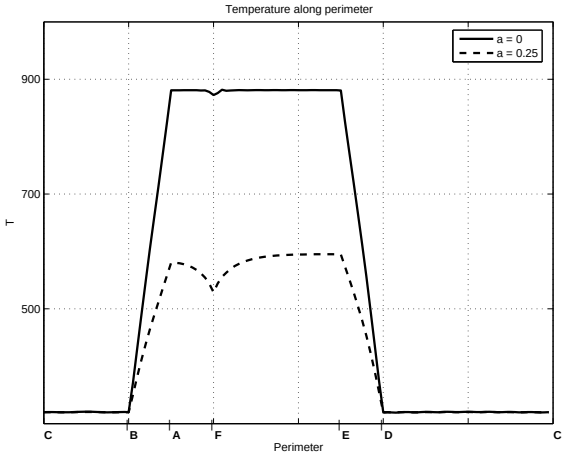

Figure 9: The boundary temperature along the perimeter of the L-shaped domain in the cases $a=0$ and $a=0.25$.

In Fig. 9, we present the boundary temperature along the perimeter of the $L-$shaped domain starting from the origin and oriented clockwise in the cases $a=0$ and $a=0.25$ and obtained using $N=M=32$. From the physical point of view, the boundary temperature distribution has an expected monotonic variation on the insulated parts of the heat conductor. This figure compares well with the corresponding figure from Bialecki and Nowak [3] obtained using the BEM.

In Figs. 10 and 11, we present the profiles of the heat flux for the cases $a=0$ and $a=0.25$, respectively, obtained using $N=M=32$. These profiles agree well with the corresponding results of Bialecki and Nowak [3] obtained using the BEM.

Finally, in Fig. 12, we present the maximum error in the boundary conditions calculated at 60 uniformly spaced boundary points, for $N=4,8,16$ and 32, in the cases $a=0,0.25$. As can be observed from these plots, the rate of convergence of the error diminishes considerably as we go from $a=0$ to $a=0.25$. In Fig. 13, we present the corresponding maximum error in the boundary conditions calculated at 60 uniformly spaced boundary points, for $N=4,8,16$ and 20, in the cases when $M=N$, $M=2N$, $M=3N$ for $a=0$. This plot indicates that there is little gain in accuracy when $M>N$.

4.3 Example 3

We finally consider a three dimensional benchmark test example with analytical solution

$$T(x_1,x_2,x_3)=4(-1+\sqrt{1+x_1+x_2+x_3}),\quad (x_1,x_2,x_3)\in(0,1)^3, \tag{4.14}$$

in a nonlinear material with thermal conductivity given by (4.10). As depicted in Fig. 14, we take $\Gamma_3=(0,1)\times(0,1)\times\{0\}$, $\Gamma_2=\emptyset$, $\Gamma_1=\partial\Omega-\Gamma_3$, $h=T_s=0$ and $R=4411500$.

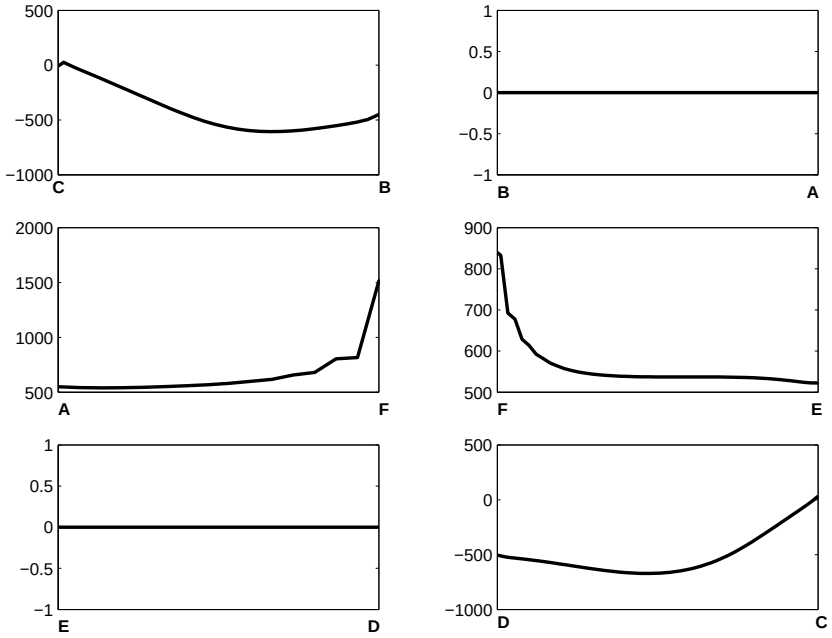

Figure 10: Profile of the heat flux along the perimeter of the L-shaped domain in the case $a=0$.

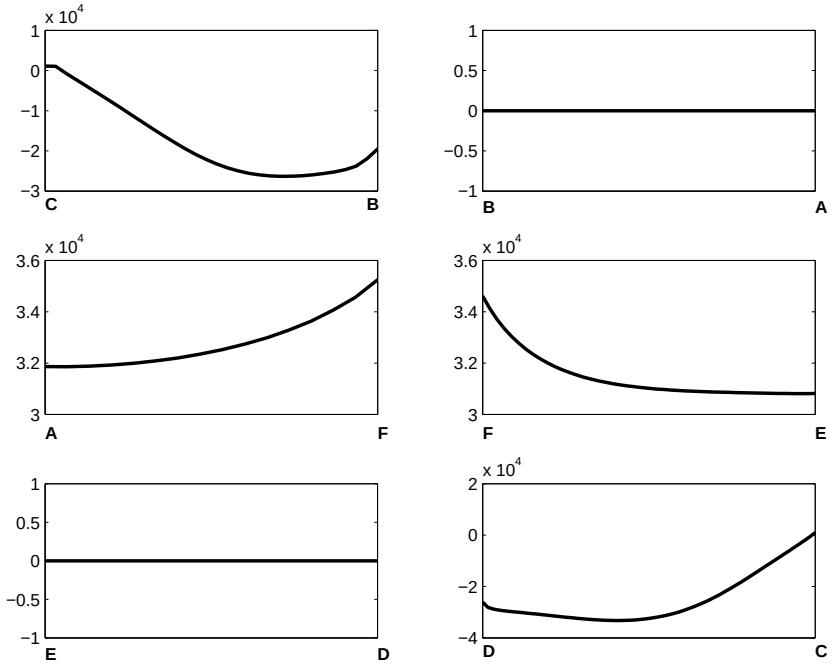

Figure 11: Profile of the heat flux along the perimeter of the L-shaped domain in the case $a=0.25$.

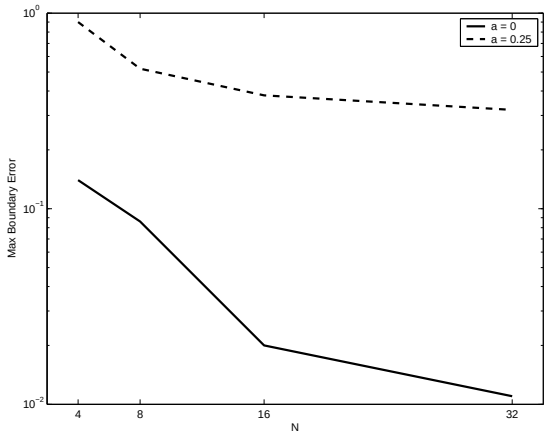

Figure 12: Maximum boundary errors with N for the cases $a=0,0.25$.

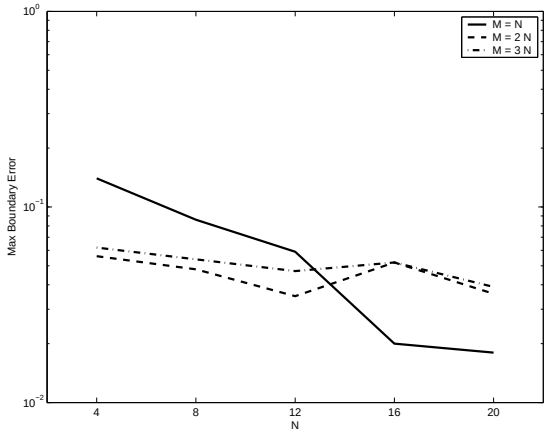

Figure 13: Maximum boundary errors with N when $a=0$ in the three cases $M=N, M=2N, M=3N$.

Based on (4.14), boundary conditions (2.2a)-(2.2c) become

$$T(0,x_2,x_3)=4(-1+\sqrt{1+x_2+x_3}),\quad T(1,x_2,x_3)=4(-1+\sqrt{2+x_2+x_3}), \tag{4.15a}$$

$$T(x_1,0,x_3)=4(-1+\sqrt{1+x_1+x_3}),\quad T(x_1,1,x_3)=4(-1+\sqrt{2+x_1+x_3}), \tag{4.15b}$$

$$T(x_1,x_2,1)=4(-1+\sqrt{2+x_1+x_3}),\quad x_1,x_2,x_3\in[0,1], \tag{4.15c}$$

$$-\left(1+\frac{T(x_1,x_2,0)}{4}\right)\frac{\partial T}{\partial x_3}(x_1,x_2,0)+T^4(x_1,x_2,0)$$
$$=-2+256\left(-1+\sqrt{1+x_1+x_2}\right)^4,\quad (x_1,x_2)\in(0,1)\times(0,1). \tag{4.15d}$$

Then (2.3) and (2.4) become

$$\Psi=\psi(T)=T+\frac{T^2}{8},\quad T=\psi^{-1}(\Psi)=4(-1+\sqrt{1+\Psi/2}). \tag{4.16}$$

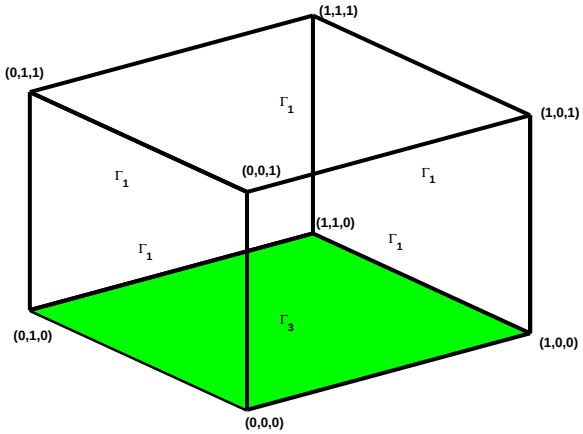

Figure 14: Geometry for Example 3.

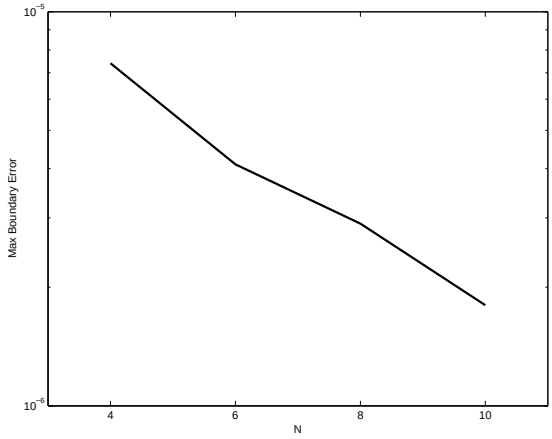

Figure 15: Maximum boundary error with N.

Based on this transformation, problem (2.5)-(2.6) becomes

$$\nabla^2\Psi(x_1,x_2,x_3)=0, \quad (x_1,x_2,x_3)\in(0,1)^3, \tag{4.17}$$

subject to the boundary conditions

$$\Psi(0,x_2,x_3)=2(x_2+x_3), \quad \Psi(1,x_2,x_3)=2(1+x_2+x_3), \quad \Psi(x_1,0,x_3)=2(x_1+x_3), \tag{4.18a}$$

$$\Psi(x_1,1,x_3)=2(1+x_1+x_3), \quad \Psi(x_1,x_2,1)=2(1+x_1+x_2), \quad x_1,x_2,x_3\in[0,1], \tag{4.18b}$$

$$-\frac{\partial\Psi}{\partial x_3}(x_1,x_2,0)+256\left(-1+\sqrt{1+\Psi(x_1,x_2,0)/2}\right)^4$$
$$=-2+256\left(-1+\sqrt{1+x_1+x_2}\right)^4, \quad (x_1,x_2)\in(0,1)\times(0,1). \tag{4.18c}$$

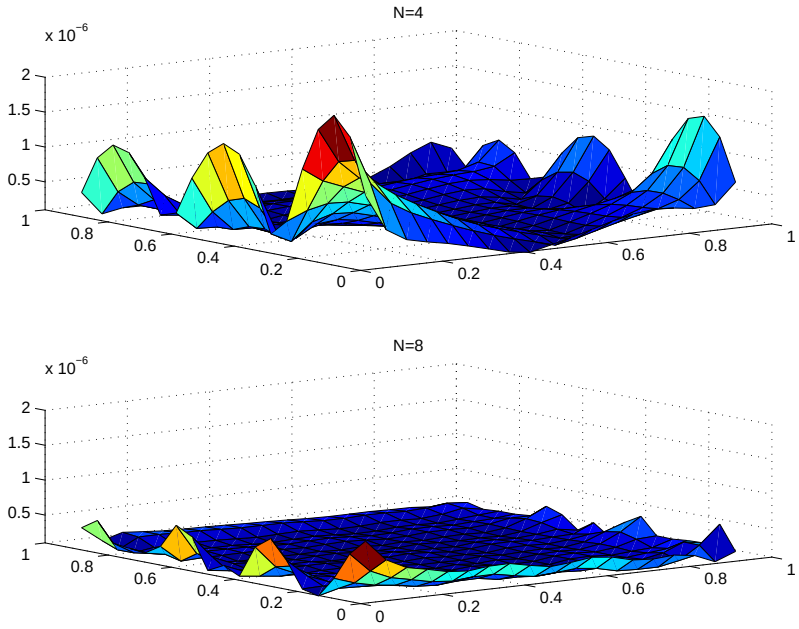

Figure 16: Error in temperature on Γ_3.

We choose $M\times M$ uniformly distributed collocation points on each of the faces of the cube and similarly $N\times N$ uniformly distributed sources on the pseudo-boundary. Thus, in this case $\mathcal{M}=6M^2$ and $\mathcal{N}=6N^2$. The maximum error (i.e., the difference between the (known) exact and the approximate solution) was calculated on a uniform 0.1×0.1 grid on each face of the cube and the maximum of these errors was recorded. In Fig. 15 we present the plot of this maximum boundary error versus N, in the case $M=N$. In Fig. 16, we present the error in the temperature on a 0.05×0.05 grid on the face Γ_3 for $N=M=4$ and $N=M=8$. From these figures it can be seen that as $M=N$ increases, the accuracy of the MFS numerical solution increases.

5 Conclusions

In this paper, the application of the MFS to nonlinear steady-state heat conduction problems was investigated. The method recasts the problem as a nonlinear minimization problem. The coefficients of the Jacobian matrix were calculated analytically resulting in substantial savings in the computational cost compared to the minimization based on finite differences. The proposed method was tested on several numerical examples. The numerical results for the two-dimensional case were found to be in good agreement with the corresponding BEM results of Bialecki and Nowak [3] showing high accuracy and stable convergence. However, unlike the BEM, the MFS can easily be extended to three-dimensional nonlinear steady-state heat conduction problems. Furthermore, al-

though the numerical examples were presented for simple geometries (square, L-shaped domain, cube), which are presumably quite adapted to standard FDM, unlike the FDM and also the FEM, the MFS can easily deal with complex irregular domains since no domain discretization is necessary. As a result, the MFS is easy to implement and requires little data preparation. Moreover, if a heat source is present in Eq. (2.1), then one may apply a modification of the MFS, as described in Golberg [9]. Future work will involve the development of the MFS for nonlinear composite materials and comparison with the corresponding BEM described in Bialecki and Kuhn [4].

Acknowledgments

The financial support received from the Royal Society for this research work is gratefully acknowledged. Parts of this work were undertaken while the first author was visiting the Department of Applied Mathematics of the University of Leeds. The authors wish to thank the two anonymous referees for their constructive suggestions.

References

[1] M. R. Akella and G. R. Kotamraju, Trefftz indirect method applied to nonlinear potential problems, Eng. Anal. Boundary Elements, 24 (2000), 459-465.
[2] J.P.S. Azevedo and L. C. Wrobel, Non-linear heat conduction in composite bodies: A boundary element formulation, Int. J. Numer. Meth. Eng., 26 (1988), 19-38.
[3] R. Bialecki and A. J. Nowak, Boundary value problems in heat conduction with nonlinear material and nonlinear boundary conditions, Appl. Math. Modelling, 5 (1981), 417-421.
[4] R. Bialecki and G. Kuhn, Boundary element solution of heat conduction problems in multizone bodies of non-linear material, Int. J. Numer. Meth. Eng., 36 (1993), 799-809.
[5] A. Bogomolny, Fundamental solutions method for elliptic boundary value problems, SIAM J. Numer. Anal., 22 (1985), 644-669.
[6] G. Fairweather and A. Karageorghis, The method of fundamental solutions for elliptic boundary value problems, Adv. Comput. Math., 9 (1998), 69-95.
[7] G. Fairweather, A. Karageorghis and P. A. Martin, The method of fundamental solutions for scattering and radiation problems, Eng. Anal. Boundary Elements, 27 (2003), 759-769.
[8] B. S. Garbow, K. E. Hillstrom and J. J. Moré, MINPACK Project, Argonne National Laboratory, 1980.
[9] M. A. Golberg, The method of fundamental solutions for Poisson's equation, Eng. Anal. Boundary Elements, 16 (1995),205-213.
[10] M. A. Golberg and C. S. Chen, The method of fundamental solutions for potential, Helmholtz and diffusion problems, in Boundary Integral Methods: Numerical and Mathematical Aspects, vol. 1 of Comput. Eng., WIT Press/Comput. Mech. Publ., Boston, MA, 1999, 103–176.
[11] P. Gorzelańczyk and J. A. Kołodziej, Some remarks concerning the shape of the source contour with application of the method of fundamental solutions to elastic torsion of prismatic rods, Eng. Anal. Boundary Elements, 32 (2008), 64-75.

[12] D. B. Ingham, P. J. Heggs and M. Manzoor, Boundary integral equation solution of non-linear plane potential problems, IMA J. Numer. Anal., 1 (1981), 415-426.
[13] R. L. Johnston and G. Fairweather, The method of fundamental solutions for problems in potential flow, Appl. Math. Modelling, 8 (1984), 265-270.
[14] A. Karageorghis and G. Fairweather, The method of fundamental solutions for the solution of nonlinear plane potential problems, IMA J. Numer. Anal., 9 (1989), 231-242.
[15] M. Katsurada, Asymptotic error analysis of the charge simulation method in a Jordan region with an analytic boundary, J. Fac. Sci. Univ. Tokyo, Sect. IA Math., 37 (1990), 635-657.
[16] M. Katsurada and H. Okamoto, The collocation points of the fundamental solution method for potential problems, Comput. Math. Applic., 31 (1996), 123-137.
[17] T. Kitagawa, Asymptotic stability of the fundamental solution method, J. Comput. Appl. Math., 38 (1991), 263-269.
[18] V. D. Kupradze and M. A. Aleksidze, The method of functional equations for the approximate solution of certain boundary value problems, USSR Comput. Math. Math. Phys., 4 (1964), 82-126.
[19] X. Li, On the convergence of the method of fundamental solutions for solving the Dirichlet problem of Poisson's equation, Adv. Comput. Math., 23 (2006), 265-277.
[20] R. Mathon and R. L. Johnston, The approximate solution of elliptic boundary-value problems by fundamental solutions, SIAM J. Numer. Anal., 14 (1977), 638-650.
[21] P. Mitic and Y. F. Rashed, Convergence and stability of the method of meshless fundamental solutions using an array of randomly distributed sources, Emg. Anal. Boundary Elements, 28 (2004), 143-153.
[22] M. N. Özişik, Boundary Value Problems of Heat Conduction, International Textbook, Scranton, 1968.
[23] K. Ruotsalainen and W. Wendland, On the boundary element method for some nonlinear boundary value problems, Numer. Math., 53 (1988), 299-314.
[24] P. A. Ramachandran, Method of fundamental solutions: singular value decomposition analysis, Commun. Numer. Meth. Eng., 18 (2002), 789-801.
[25] G. Rus and R. Gallego, Optimization algorithms for identification inverse problems with the boundary element method, Eng. Anal. Boundary Elements, 26 (2002), 315-327.
[26] Y.-S. Smyrlis and A. Karageorghis, Some aspects of the method of fundamental solutions for certain harmonic problems, J. Sci. Computing, 16 (2001), 341-371.
[27] R. Tankelevich, G. Fairweather, A. Karageorghis and Y.-S. Smyrlis, Potential field based geometric modelling using the method of fundamental solutions, Int. J. Numer. Meth. Eng., 68 (2006), 1257-1280.
[28] Th. Tsangaris, Y.-S. Smyrlis and A. Karageorghis, Numerical analysis of the method of fundamental solutions for harmonic problems in annular domains, Numer. Meth. Partial Diff. Eqns., 22 (2006), 507-539.